Emerging investigator series: Synthesis of Magnesium Oxide Nanoparticles Fabricated on Graphene Oxide Nanocomposite for CO2 Sequestration at Elevated Temperatures

Article *in* Environmental science. Nano · February 2020

DOI: 10.1039/C9EN01442J

CITATIONS
6

READS
96

8 authors, including:

Chamila Gunathilake
Home
44 PUBLICATIONS **668** CITATIONS
SEE PROFILE

Tharindu Ranathunge
University of Mississippi
17 PUBLICATIONS **33** CITATIONS
SEE PROFILE

Rohan Dassanayake
University of Sri Jayewardenepura
45 PUBLICATIONS **440** CITATIONS
SEE PROFILE

Sachintha D Illesinghe
University of Sri Jayewardenepura
2 PUBLICATIONS **6** CITATIONS
SEE PROFILE

View Article Online
View Journal

Environmental Science Nano

Accepted Manuscript

This article can be cited before page numbers have been issued, to do this please use: C. Gunathilake, G.G.T.A. Ranathungea, R. Dassanayake, S. D. Illesinghe, A. Manchanda, C. S. Kalpage, R. M. G. Rajapakse and D. G. G. P. Karunaratne, *Environ. Sci.: Nano*, 2020, DOI: 10.1039/C9EN01442J.

ROYAL SOCIETY OF CHEMISTRY

rsc.li/es-nano

View Article Online
DOI: 10.1039/C9EN01442J

Environmental Significance Statement

Atmospheric concentration of CO_2 reached a maximum of 410 ppm in 2019 April, which is the highest reported value ever since measurements began. According to the EPA, such greenhouse gas emissions can cause a 2-4 ^oC increase in temperature during the next century if CO_2 atmospheric levels are not reduced. Although this change may appear insignificant, it is projected to cause extreme weather disasters, such as droughts and floods; threaten coastal resources and wetlands by raising sea level; and increase the risk of certain diseases by producing new breeding sites for pests and pathogens. The degradation of the natural ecosystem could furthermore lead to reduced biological diversity. Thus, it is very important to diminish this excessive CO_2 concentration in atmosphere using more energy efficient, economically feasible and environmentally friendly techniques

Thus, magnesium oxide nanoparticles (MONPs) and MONP fabricated graphene oxides (MONP-GOs) were synthesized using sol-gel method and applied for CO_2 sorption indicate that these samples were shown to be good sorbents for CO_2 capture (displaying a significantly high CO_2 uptake of 2.79-3.34 mmol/g) at two different elevated temperatures ((60 and 120 ^oC) through the chemisorption mechanism. These materials display high affinity toward CO_2 sorption at 60 and 120 ^oC . High sorption capacity at elevated temperatures, preferential selectivity, low cost of these sorbents along with chemical and mechanical stability of MONPs and MONP are the remaining factors that determined before their commercial application for CO_2 capture.

DOI: 10.1039/C9EN01442D

ARTICLE TYPE www.rsc.org/xxxxxx | XXXXXXXX

Emerging investigator series: Synthesis of Magnesium Oxide Nanoparticles Fabricated on Graphene Oxide Nanocomposite for CO_2 Sequestration at Elevated Temperatures

C. A. Gunathilake,[a,*] G. G. T. A. Ranathunge,[b] Rohan S. Dassanayake,[c,d] S. D. Illesinghe,[e] Amanpreet, S. Manchanda,[f] C. S. Kalpage,[a] R. M. G. Rajapakse,[b] D. G. G. P. Karunaratne.[a]

Received Xth XXXXX 20XX, Accepted Xth XXXXX 20XX
First published on the web Xth XXXXX 20XX
DOI: 10.1039/xxxxxxxx

Incorporation of alkaline metal oxides into porous templates is considered a novel chemisorbents for capturing greenhouse gases including CO_2 at elevated temperatures. Thus, magnesium oxide nanoparticles (MONPs) and MONP fabricated graphene oxides (MONP-GOs) were synthesized using the sol-gel method. Preparation of these materials was carried out by a three-step facile synthesis route involving: (1) synthesis of magnesium oxide (MO) nanoparticles (MONPs), (2) synthesis of graphene oxide (GO) from commercially available graphene, and (3) incorporation of MONPs on graphene oxide. Both MONP and MONP-GO samples exhibited a significantly high CO_2 uptake of 2.79-3.34 mmol/g at two different elevated temperatures (60 and 120 ^oC). The increased CO_2 adsorption is due to the presence of terminal OH groups and acid-base pair sites at magnesium (Mg^{2+}-O^{2-}) surface in MONP and MONP-GO materials, respectively, resulting in the formation of hydrogen carbonate species and bidentate carbonate complexes with CO_2 gas. Our composite material also possesses intriguing properties including high thermal and chemical stabilities, low-cost, and environmental benignity along with its enhanced CO_2 sorption making it an excellent candidate for CO_2 capture in fossil fuel-based power plants at elevated temperatures.

Introduction

In the recent past, human activities have caused excessive damage to the environment resulting in unpredictable climate patterns. Greenhouse gases (GHG) including carbon dioxide (CO_2), chlorofluorohydrocarbon (CFCs), nitrous oxide (NO_x), methane (CH_4), ozone (O_3), and water vapor are major examples of industrial products that disrupt the earth's tropospheric equilibrium. CO_2, a major greenhouse gas, is released into the environment via fossil fuel consumption, volcanic eruptions, coal burning in industry, forest fires, and industrial missions. The atmospheric concentration of CO_2 reached a maximum of 410 ppm in 2019 April, which is the highest reported value ever since measurements began.[1]

The most effective approach to address the increasing CO_2 emissions is to reduce fossil fuel consumption or to use catalytic converters and filters that can adsorb CO_2. CO_2 capture and sequestration (CCS) is a currently available technology that utilize to minimize CO_2 emissions from coal and gas-fired power plants, industrial processes, and other stationary sources of CO_2. CCS technologies are responsible for capturing CO_2 up to 90% of emissions produced from the burning of fossil fuels during the generation of electricity and various other industrial processes.

Current CO_2 capturing technologies are mainly based on liquid-based chemical sorbents. Heating and depressurization techniques are commonly used to regenerate the adsorbed CO_2. Industrial power plants capture CO_2 by aqueous amine-based solutions such as diethanolamine (DEA), diglycolamine (DGA), monoethanolamine (MEA), and their derivatives including N-methyldiethanolamine (NMDEA)[2, 3]. However, the potential amine group degradation is one of the major challenges of utilizing these amine-based liquid sorbents for large-scale CO_2 capture and sequestration. Amines show low chemical stability and selectivity for CO_2 in the presence of other oxidizing gases such as nitrogen dioxide (NO_2), nitrous oxide and (NO), sulfur dioxide (SO_2), and degrade to harmful nitrosamines and nitramine products [4, 5]. Other setbacks of

[a]*Department of Chemical and Processing Engineering, Faculty of Engineering, University of Peradeniya, 20400, Sri Lanka*
[b]*Department of Chemistry, University of Peradeniya, 20400, Sri Lanka*
[c]*Department of Chemistry, Ithaca College, Ithaca, NY, 14850, USA.*
[d]*Department of Biosystems Technology, Faculty of Technology, University of Sri Jayewardenepura, Gangodawila, Nugegoda, 10250, Sri Lanka*
[e]*Department of Forestry and Environmental Sciences, University of Sri Jayawardhanapura, Gangodawila, Nugegoda, 10250, Sri Lanka.*
[f]*Department of Chemistry, California State University Stanislaus, One University Circle, Turlock, California, 95382, USA.*

* *Corresponding Author: Department of Chemical & Process Engineering, Faculty of Engineering, University of Peradeniya, Peradeniya, Sri Lanka. Tel.: +94718311117*
E-mail address: chamilag@pdn.ac.lk
† Electronic Supplementary Information (ESI) available: [Room temperature CO_2 adsorption measurements, CO_2 chemisorption, TPD measurements, Characterization, and Calculations]. See DOI: 10.1039/xxxxxx/.

View Article Online
DOI: 10.1039/C9EN01442J

this technology also include solvent loss, energy extensive CO_2 regeneration and, corrosion.

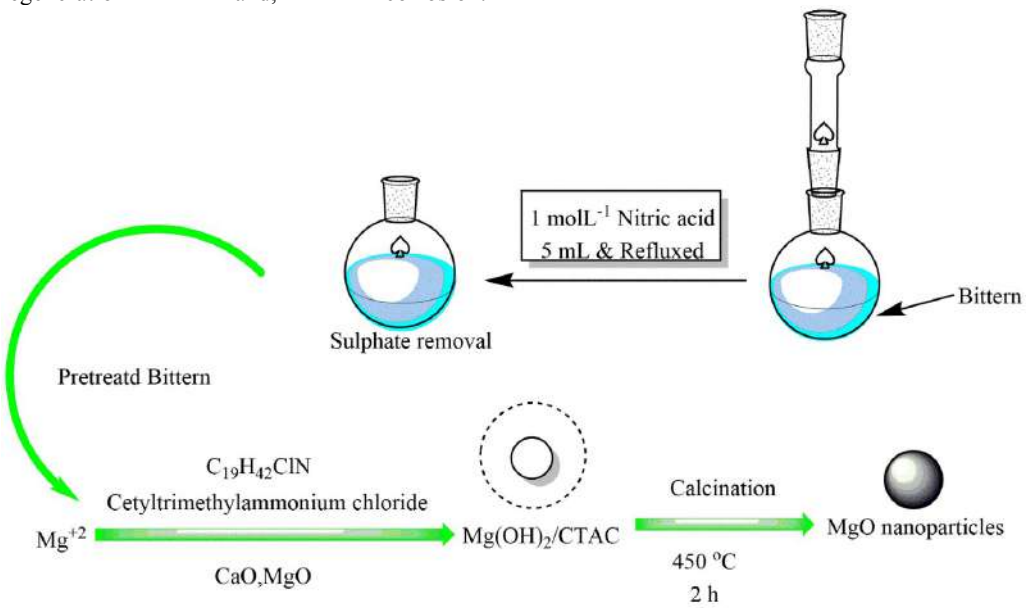

Scheme 1. Pre-treatment of Bittern and synthesis of MONP (MgO Nanoparticles)

Therefore, it is imperative to control the CO_2 emissions using more energy-efficient, economically feasible and environmentally friendly techniques.

The amine-scrubbing process is another technique to capture CO_2 by the physisorption [6]. However, this technique also suffers from major disadvantages such as relatively low thermal stability of amines and high energy requirement to regenerate CO_2. Recently, as an alternative to the liquid amine sorption, solid sorbents have been introduced for the sorption of CO_2 from flue gas streams due to their distinct properties including high sorption and selectivity, less energy consumption for CO_2 regeneration, and relatively easy handling. Even though CO_2 capturing involves both physical or chemical solid sorbents via physical adsorption or chemisorption, chemisorption-based processes show higher selectivity and high CO_2 sorption capacity over physisorption-based processes at temperatures above 40 °C [7, 8].

MONPs (magnesium oxide nanoparticles) have been widely investigated for preparing anti-microbial agents,[9], heat-resistant and mechanically strength materials[10], chromatographic membranes [11], organic light-emitting diodes (OLEDs) [12], reactive catalysts [13], dye-sensitized solar cells [14] and coating agents of furnaces [15]. However, the methods employed for magnesium oxide nanoparticles synthesis are expensive and inefficient [16-18]. So, there is a great need for developing novel and inexpensive methods to synthesize MONPs. In this study, we report the use of bittern, a by-product and a waste produced in large quantities from industries such as salt and dolomite mining, as our magnesium sources. These sources were subsequently converted into pure MONP, providing an additional value to industrial waste and addressing disposal concerns of the bittern. The sol-gel process is widely reported for synthesizing MONPs [19, 20]. It has also been reported that the surface morphology and homogeneity of MONPs can be improved using surfactants as soft templates in the sol-gel process [21]. For example, Mastuli et al. reported the use of a cationic surfactant in the sol-gel synthesis of MONPs [22]. Alternatively, the synthesis of nanocrystalline MgO particles by combustion followed by annealing using hexamine as a fuel has been described by Balamurugan et al. [23]. These MONPs have terminal hydroxyl groups, which can be chemically bonded to carbon dioxide. Hence, CO_2 possibly forms hydrogen carbonate species and bidentate carbonate complexes with MONPs.

Graphite is a covalent carbon system with a hexagonally bonded cyclic lattice consist of multilayers. When graphite is oxidized to graphene oxide (GO) by strong oxidizing agents [24], oxygenated functionalities such as hydroxy, epoxy, and carbonyl groups are introduced into the structure of the graphite, giving more hydrophilic nature and layer separation [25, 26]. The oxygenated functionalities in GO can strongly affect its mechanical, electronic, and electrochemical properties[27]. The presence of these functional groups can also provide potential advantages of using GO in numerous applications including, catalysis, adsorption, electrochemical, and sensors.[26,28-30] GO is an excellent adsorbent as it can be chemically, thermally, or electrochemically engineered, giving high surface properties [24, 27, 31]. Due to its tunable morphology, GO has been widely used for the preparation of composite materials with metal-organic frameworks (MOF), metals, and metal oxides [26, 28, 29, 32]. GO-based composite materials have recently attracted attention as sorbents for CO_2 adsorption. For instance, Bhanja et al. demonstrated the CO_2 storage capacity of 8.10 mmol/g and 2.10 mmol/g at 0 and 25 °C,

View Article Online
DOI: 10.1039/C9EN01442J

respectively, for imine-functionalized graphene oxide (IFGO)[33]. Pokhrel and co-workers investigated the CO_2 adsorption capacity and kinetics of composite materials prepared from graphene oxide (GO),

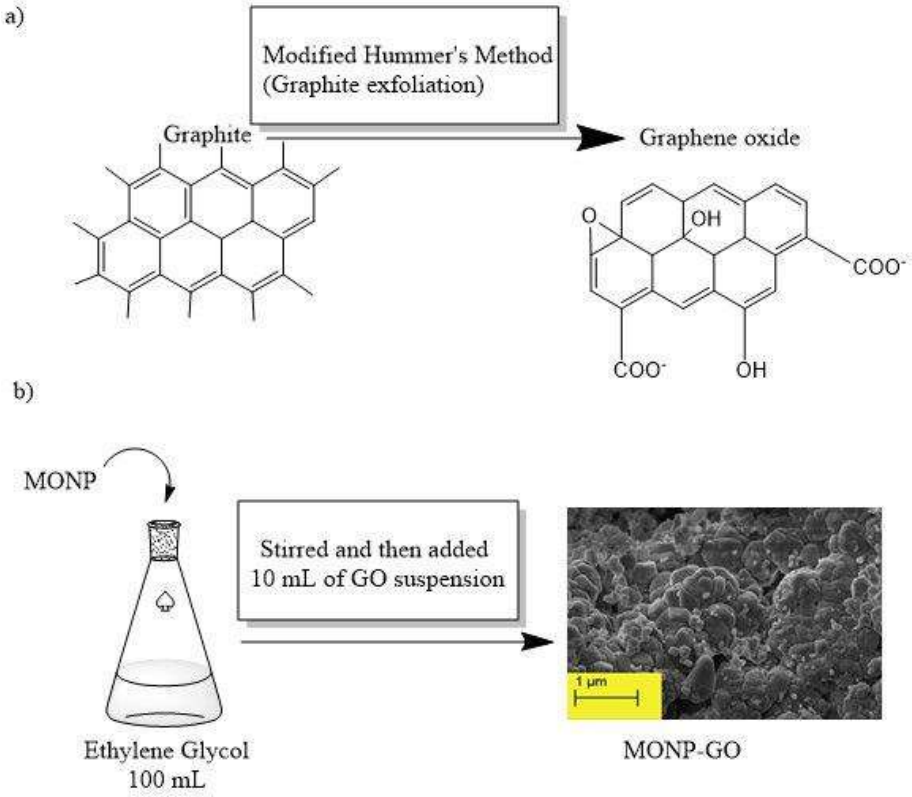

Scheme 2. a) Preparation of GO (using modified hummer's method) and b) preparation of MONP-GO

zeolitic imidazolate framework ZIF-8, and composite ZIF-8/GO adsorbents with various amine functionalities including 3-aminopropyl-triethoxysilane (APTES), polyethyleneimine (PEI), and ethylenediamine (ED)[26]. Zhou et al. reported the CO_2 capture performance of ethylenediamine (EDA)-functionalized graphene oxide (GO) hollow fiber membranes with CO_2 permeance of 660 GPU and CO_2/N_2 selectivity of > 500 at 75 °C [34]. Alghamdi and co-workers showed the highest CO_2 adsorption capacity of 1.36 mmol/g for their activated nitrogen-doped graphene oxide sheets prepared from polypyrrole doped with C_6H_5-SO_3-K at 50 °C and 1.0 atm [35]. Yang et al, synthesized graphene-based mesoporous silica sheets Impregnated with polyethyleneimine and displayed CO_2 adsorption capacity of 4.32 mmol/g with cycle ability at 75 °C.[36]

Herein, we report the facile and low-cost synthesis of MONPs and MONPs fabricated on GO using the sol-gel method in the presence of an ethylene glycol-water molecular template. All materials were synthesized from low-cost and naturally existing graphite, bittern, and dolomite. Both MONPs and MONP-GO nanocomposites were investigated for CO_2 gas adsorption at low (0 ºC), room (25 ºC) and elevated temperatures (60 and 120 ºC). To the best of our knowledge, this is the first attempt to utilize an ethylene glycol-water molecular template to synthesize MONP-GO nanocomposites for CO_2 capture, especially at elevated temperatures (T>50 ºC).

Experimental

Materials

Cetyltrimethylammonium chloride (CTAC) (98%), nitric acid (68% V/V) and barium chloride ($BaCl_2$) (99%) were purchased from Sigma-Aldrich, ethylene glycol (EG) (98% purity), potassium permanganate ($KMnO_4$) (99% assay), sulfuric acid (H_2SO_4) (98% assay), sodium nitrate ($NaNO_3$) (98% assay), hydrogen peroxide (H_2O_2) (40% assay), and hydrochloric acid (HCl) (37% assay), were purchased from BASF and used without further purification. Bittern was collected from Puttalam salt Ltd., Palavi, Puttalam, Sri Lanka (N 7.979826°, E 79.828478°) was used as magnesium sources and these materials were characterized by their specific gravity using the ASTM standard (D1429) hydrometer method [37]. The solutions of specific gravity > 1.25 were used for the synthesis purpose [38]. For a 200 mL bittern solution, 5.0 mL of 1.0 M HNO_3 was added and the solution was refluxed for 1 h until completely soluble. The solution was then treated with 0.50 M $BaCl_2$ to remove sulfate ions. After the completion of precipitation, the suspension was filtered, and the clear filtrate was collected.
As the secondary magnesium source, dolomite obtained from

View Article Online
DOI: 10.1039/C9EN01442J

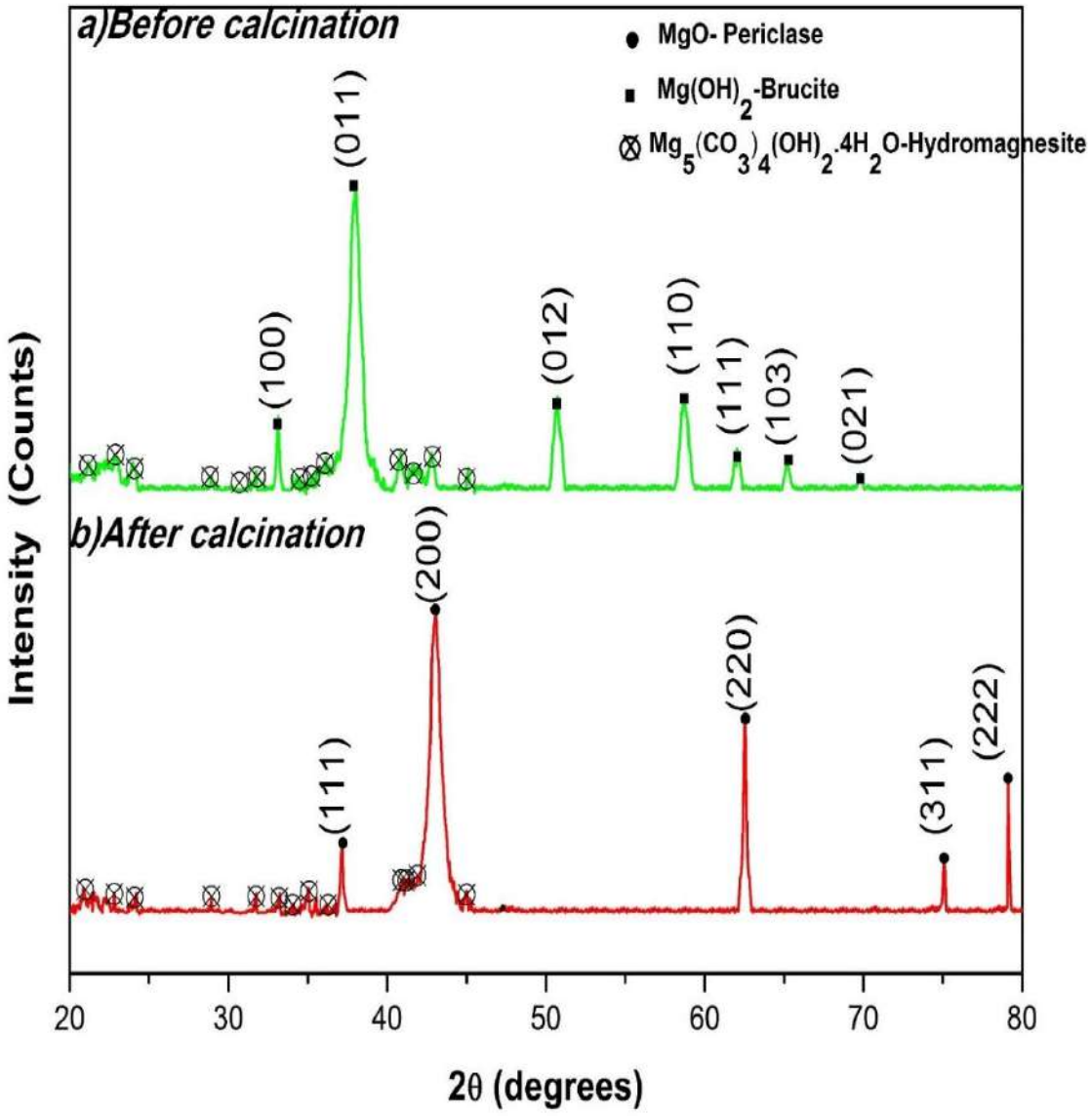

marble quarry (collected from Madawala Ulpatha, Nalanda,

Figure 1. XRD pattern of a) Before calcination and b) After calcination of MONPs.

Sri Lanka (N 7.573308°, E 80.626237°)) was also used. A 15.0 g of dolomite was crushed and grounded in a sintered crucible. The powdered sample was then sieved to obtain particles with a size less than 150 µm. These particles were heated at 1000 °C for 2h to produce calcined dolomite

Synthesis

Preparation of Magnesium Oxide Nanoparticles (MONPs)

MONPs were synthesized using a sol-gel method (see Scheme 1). First, a 100.0 mL of pre-treated bittern solution was poured into a beaker and a 1.00 mL of 1 mM CTAC surfactant was then added and stirred for 1 h. 2.00 g of calcined dolomite was then slowly added to the reaction mixture and thoroughly stirred for 12 h. The undissolved part settled at the bottom of the beaker while the gel remained in the upper portion. The gel was separated and heated in an oven at 100 °C for 24 h. The dry powder was washed several times with distilled water and 5% ethanol. Then the powder was dried and calcined at 450 °C for 2 h in a furnace to obtain final MONPs.

Preparation of Graphene Oxide (GO)

Graphite was obtained from the natural veins of Sri Lanka. Initially, it was ball milled and sieved to 45 µm. After that, 4.00 g of graphite flakes and 2.40 g of $NaNO_3$ and 120 mL of H_2SO_4 (98 wt.%) were mixed in a 1000 mL volumetric flask at 6 °C in an ice bath under constant stirring. The sample mixture was further stirred for additional 2 h at 6 °C

View Article Online
DOI: 10.1039/C9EN01442J

while slowly adding 15.00 g of $KMnO_4$. Then the mixture was stirred at 35 °C for 30 min until it became a brownish color paste. The mixture was sonicated for 5 min and this step was repeated 12 times. Next, the reaction was quenched by slowly adding 230 mL of distilled water. During this step, the temperature of the reaction mixture was increased quickly to 96 °C and the color of the mixture also turned to brown. The complete termination of the oxidation by $KMnO_4$ was achieved with the addition of 8 mL H_2O_2 under constant stirring (see in Scheme 2a for the conversion of graphite into GO). After that, the color of the solution was turned into yellow. For further purification, the mixture was washed by centrifugation, followed by rinsing with 8% HCl and deionized (DI) water for numerous times until the supernatant becomes neutral. The suspension was filtered and dried at 50 °C to obtain powdered GO.

Preparation of Magnesium Oxide Nanoparticles Fabricated Graphene Oxide (MONP-GO)

A 0.20 g of previously synthesized MONPs was added to a 100 mL of ethylene glycol (EG) and stirred for 5 h (see Scheme 2b). Then a GO suspension in ethylene glycol was prepared separately using a 1.20 g of GO powder mixing with 1 mL of distilled water and 9 mL of ethylene glycol. The prepared GO/EG suspension was carefully added to the MONP mixture and stirred for 12 h. Next, the suspension was centrifuged for 5 min at 8000 rpm and the composite was collected. The collected residue was dried at 50 °C overnight. Note that the notations MONPs and MONP-GO represent the magnesium oxide nanoparticles and magnesium oxide nanoparticles fabricated on graphene oxide, respectively.

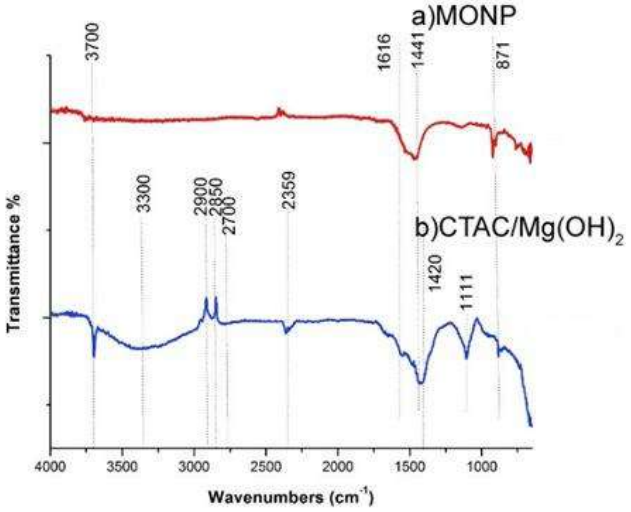

Figure 2. FTIR spectra of (a) MONP (top) and (b) CTAC/$Mg(OH)_2$ (bottom).

Characterization

All samples were characterized using Fourier transform infrared spectroscopy (FTIR), thermogravimetry (TGA), X-ray powder diffraction (XRD) analysis, nitrogen sorption, scanning electron microscope (SEM), energy diffractive X-ray (EDX), and particle size analyzer (PSA). Techniques pertaining to the characterization of MONPs and MONP-GO structures are included in the Electronic Supporting Information (ESI).

Calculations CO_2 physisorption at 0 and 25 °C

The procedure used for the CO_2 adsorption experiment was analogous to the previously reported method elsewhere [39]. A detailed description of the procedure is included in the ESI.

CO_2 chemisorption at elevated temperatures (60 °C and 120 °C)

The procedure tested for the CO_2 chemisorption and TPD (Temperature Programmed Desorption) measurements was similar to the previously described method [39]. A detailed procedure for the above measurements is included in the ESI.

Results and Discussion

Synthesis of magnesium oxide nanoparticles (MONPs)

In this synthesis, magnesium ions react with hydroxyl ions to form magnesium hydroxide ($Mg(OH_2)$) particles which then nucleate within the cavities of soft templates formed by cetyltrimethylammonium (CTAB) ions. These nuclei grow up to a certain size determined by the cavity size along with other factors including interactions between the surfactants and $Mg(OH_2)$ particles formed, and surface coverage. Calcination of $Mg(OH_2)$ gel leads to the formation of MONPs. The X-ray diffractograms of the products before and after the calcination process are shown in Figure 1 top (a) and bottom panel (b), respectively.

The XRD pattern obtained before the calcination process mainly comprised of $Mg(OH_2)$ (see Figure 1a). Diffraction peaks at 33.0°, 37.9°, 50.8°, 58.5°, 62.0°, 65.2° and 69.8° for $Mg(OH_2)$ are ascribed to crystallography planes of (100), (011), (012), (110), (111), (103) and (021), respectively. All these peaks are consistent with the XRD patterns reported for the brucite crystalline form of $Mg(OH_2)$ [40]. The major peak at 37.9° is attributed to the 011 planes, giving the average crystalline size of 5 nm. XRD peaks of calcined MgO nanoparticles appeared at 37.1°, 43.1°, 62.4°, 75.3°, and 79.5° correspond to the diffraction pattern observed from (111), (200), (220), (311) and (222) planes, respectively [41]. The crystalline size of 20.0 nm for MgO was determined using the Debye-Scherrer formula applied at 43.1°major peak of MgO. The average crystallite size of MgO is increased which could be due to the irreversible aggregation of MgO particles after the removal of surfactant molecules upon heating. The trace amounts of hydro-magnesite ($Mg_5(CO_3)_4(OH)_2.4H_2O$) present in the sample after calcination (Figure 1b) is due to the incomplete oxidization as thermal energy is insufficient to convert all magnesite to periclase.

Figure 2 shows the IR spectra of MONP and MONP with CTAC/$Mg(OH)_2$ after and before calcination. IR spectra of

View Article Online
DOI: 10.1039/C9EN01442J

MONP and MONP with CTAC/$Mg(OH)_2$ show characteristic peaks at 1441 cm^{-1} and 1616 cm^{-1} correspond to bending vibrations of O-H and Mg-O respectively [42]. Asymmetric (ν_{as}) and symmetric (ν_s) stretching vibrations of the methylene group of CTAC appear in the range of 2700 cm^{-1} to 2900 cm^{-1}. [43-44]. The presence of the tertiary amine group of CTAC terminal end is distinguished by the C-N stretching vibration in the range of 1420 to 1441 cm^{-1}. The broad peak in the range of 3300 to 3700 cm^{-1} is due to stretching vibrations of hydrogen bonding between O-H groups of magnesium hydroxide and nitrogen end terminal of CTAC molecules [45]. As can be seen from Figure 2(a) upon the removal of surfactant by calcination, the disappearance of the bands correspond to the surfactant (CTAC) is clearly observed.

Figure 3 shows SEM images of MONP at two different magnifications (a) 1 µm and (b) 200 nm. Samples display a flake-like surface morphology. The flakes have diameters in the range from 20 nm to 49 nm and widths from 80 nm to 400 nm. Particles have agglomerated to form a porous structure, subsequently enhancing the surface area of the aggregated particle units. The particle size distribution (PSD) was also measured using dynamic LASER light scattering- based Particle Size Analyser.

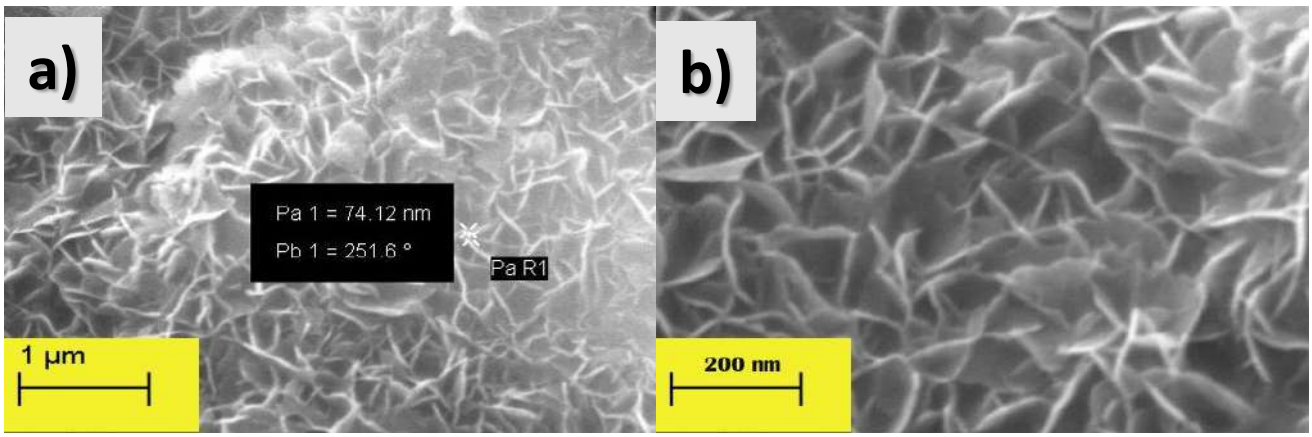

Figure 3. Surface morphology of prepared magnesium oxide nanoparticles (MONP) a) 25,000× and b) 50,000× magnifications

As shown in Figure 4, data showed a narrow distribution at 15- 40 nm and a broad distribution at 91-400 nm of particles, further suggesting the flake-like morphology of the nanoparticles synthesized. The purity of the final product was measured using EDX with 98.6 wt. % of MgO, 0.71 wt. % of NaCl and 0.69 wt. % of SiO_2.

Unlike other metal /GO composites, the synthesis of MONP-GO composite is difficult due to the high decomposition temperature of MgO (400 °C). Note that GO can be also reduced giving a black color powder with an altered structure upon heating at high temperatures. Therefore, synthesizing the MONP-GO composite with metal ions intercalation directly to the carboxyl groups and hydroxyl groups in the nanographene sheet is difficult. However, with simple electrostatic interactions at 50 °C, it is possible to connect both materials together as reported elsewhere by Lu et al, which shows the use of noncovalent decoration of graphene oxide sheets with nanocrystals [46].

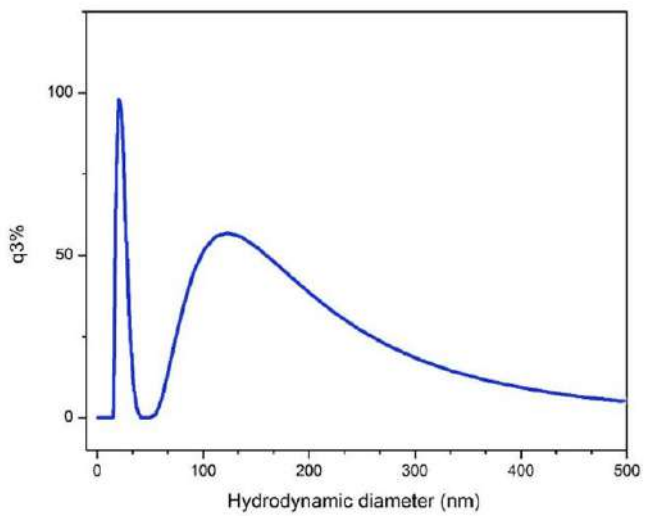

Figure 4. Particle size distribution of synthesized MONP.

The XRD pattern of the obtained MONP-GO is shown in Figure 5. Main XRD peaks appeared at 37.1°, 43.1°, and 62.4° are corresponding to (111), (200), and (220) planes in the MONP, respectively. These data agree with the standard data recorded in the JCPDS database. [JCPDS file 45-0946].

View Article Online
DOI: 10.1039/C9EN01442J

Debye-Scherrer formula can be applied to the major XRD peak at 43.1° to determine the size of the crystallite.

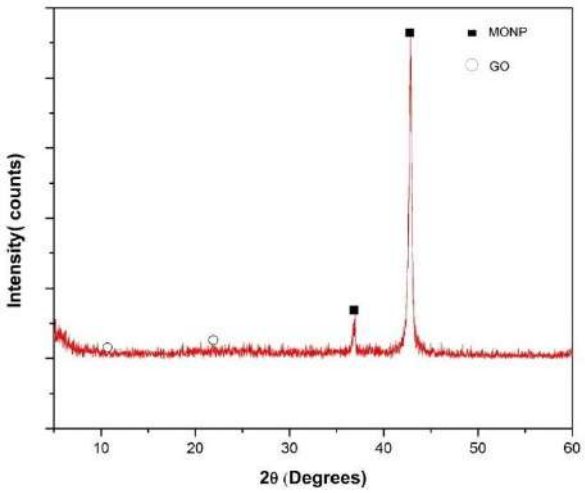

Figure 5. XRD pattern of synthesized MONP-GO nanocomposite.

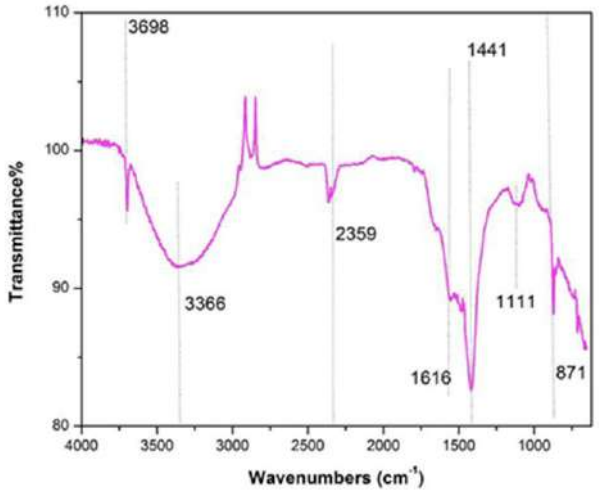

Figure 6. FTIR spectrum of MONP-GO composite.

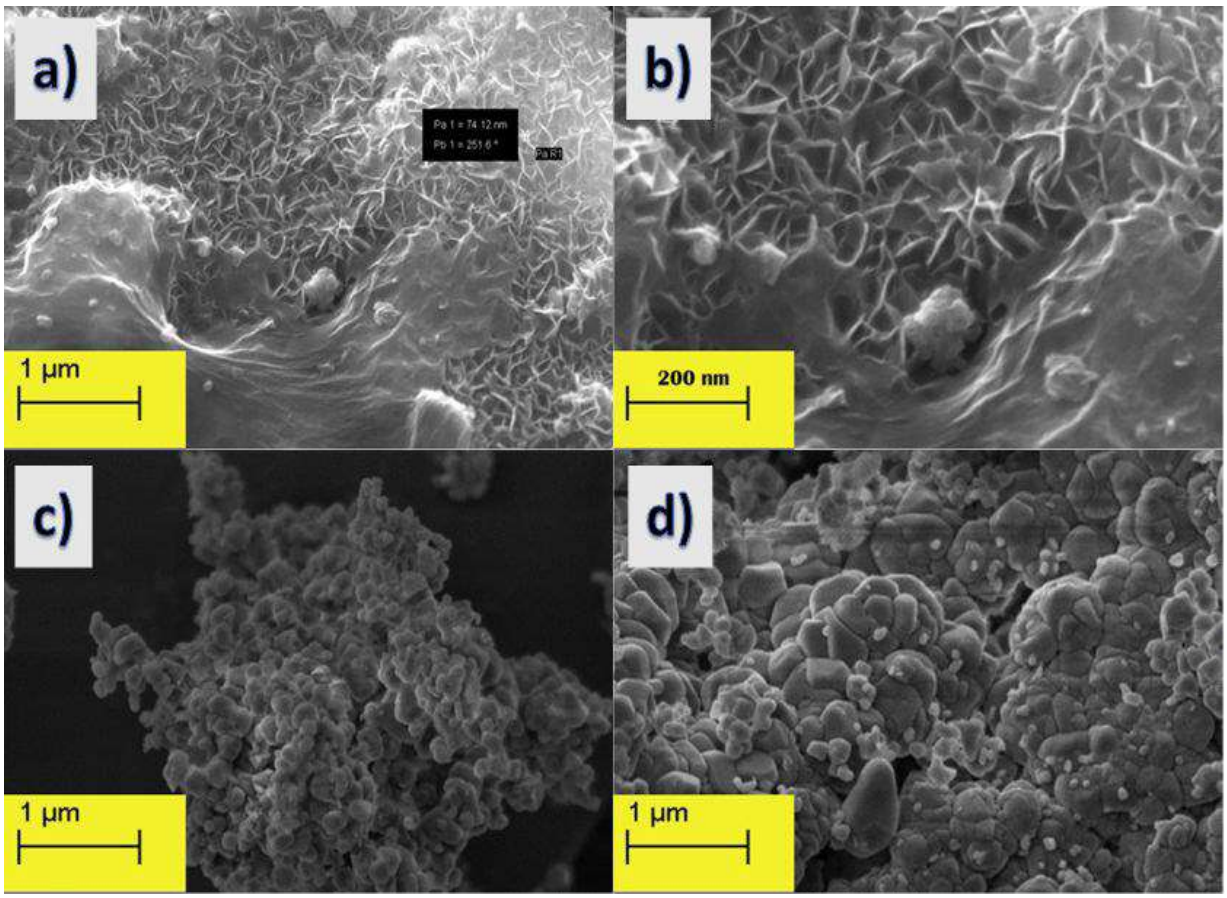

Figure 7. SEM images obtained a) after 1 h of conjugation of MgO and GO (magnification 25000 X) b) after 1 h of conjugation of MgO and GO (magnification 50000 X) c) after 12 h of stirring MONP-GO coating (magnification 25000 X), and d) after 12 h of stirring MONP-GO coating (magnification 50000 X).

View Article Online
DOI: 10.1039/C9EN01442J

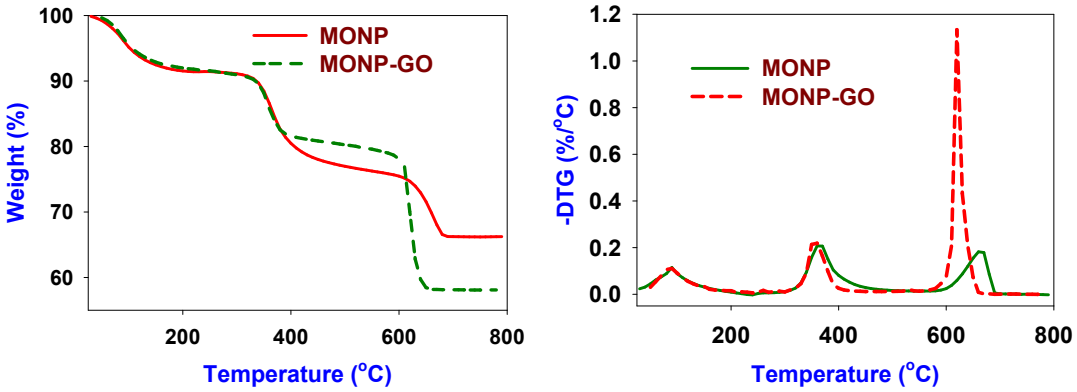

Figure 8. TG curves (left panel) and their corresponding DTG curves (right panel) recorded for the MONP and MONP-GO samples studied.

Some nanoparticles are aggregated on top of the GO layer. Due to the convolutions of the surface, a larger amount of adsorption is expected in the composite. Note that the XRD profile was taken in the 2-degree range of 5° and 60°. Therefore, the last characteristic peak of GO at 62.4° is not shown in Figure 5. GO shows two small peaks at 10° and 22.1°. Due to the amorphous nature of GO, these two peaks are not clearly visible in the XRD profile. Moreover, the amorphous nature of GO increases during the oxidation of graphene to GO, giving low intense and broad XRD peaks. [47, 48]

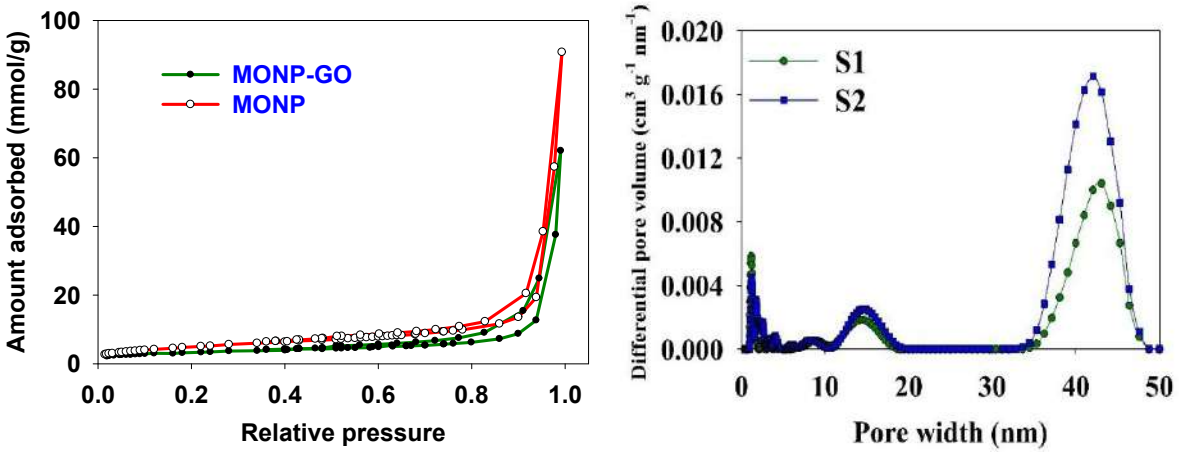

Figure 9. Adsorption isotherms (left panel) and the corresponding PSD curves (right panel) for MONP and MONP-GO samples studied; note that S1 represent the PSD of MONP and S2 represent the PSD of MONP-GO in the right panel.

The formation of MONP-GO is further confirmed by FTIR analysis. Figure 6 shows the FTIR spectrum of MONP-GO. The presence of a broad absorbance band at 3366 cm^{-1} is attributed to the –OH stretching vibrations of the hydroxyl groups of the GO. [49]. Two small shoulder peaks at ~1730 cm^{-1} and ~1630 cm^{-1} are corresponded to C=O and C=C stretching vibrations in GO. The vibration peaks at 1441 cm^{-1} and 1616 cm^{-1} correspond to the bending vibrations of –OH and –Mg–O, respectively [42]. The band at 1111 cm^{-1} is ascribed to the C-O-C stretching vibration of GO. [49] The characteristic peak at 857.87 cm^{-1} is attributed to the vibration of –Mg–O stretching bond indicating the existence of the MgO in the MONP-GO composite. [50]

The fabrication of the composite is performed at low temperatures (50-60 °C) to avoid the reduction of GO to reduced GO (RGO) [51]. Also, direct MgO nucleation through the GO texture is not possible as the thermal decomposition occurs at high temperatures.

Table 1. Adsorption parameters for the MONP and MONP-GO samples studied.

Content	V_{sp} (cc/g)	V_{mic} (cc/g)	S_{BET} (m^2/g)	W_{max} (nm)	V_t (cc/g)
MONP	0.10	<0.01	18	46	0.14
MONP-GO	0.06	<0.01	12	48	0.10

V_{sp}-single-point pore volume calculated at the relative pressure of 0.98;V_{mi}–The cumulative pore volume of micropores, (pores below 2 nm) was calculated on the basis of the PSD curves obtained by the DFT

View Article Online
DOI: 10.1039/C9EN01442J

software; S_{BET} – specific surface area calculated from adsorption data in relative pressure range 0.05-0.20; W_{max} - pore width calculated at the maximum of PSD obtained by using the 2DNLDFT Heterogeneous Surface model; V_t - total pore volume calculated by integration of the PSD curve;

In this study, ethylene glycol medium was used to synthesis nanocomposite and to overcome hydration. Previous studies by Oviedio et al and Wogelius et al show the hydration of periclase crystals to brucite[52, 53]. Recent studies by Heidarizad et al [54, 55] reported that the synthesis of GO/MgO nanocomposite encounters the issue of forming $Mg(OH)_2$. However, this issue was successfully overcome by using ethylene glycol as the medium. Ethylene glycol also acts as a soft template for the formation of nanoparticles[56]. This is due to the hydroxyl groups present in the medium assemble with magnesium to form a stabilized micelle via electrostatic interactions. In addition, GO suspension also influenced by the soft template to assure the encapsulation of GO to nanoparticles and to behave in a control morphism.

In contrast to the previous studies reported by Rui Juan et.al [57], Chen et al.[58] and Zhao et al.[59], the presence of distilled water in 4 mL of ethylene glycol suspension (water: ethylene glycol, 1:4) prevents the microsphere formation. The surface morphology (SEM images) of the synthesized compound at each step described in the synthesis procedure are shown in Figure 7. These SEM images were taken in the dry form of MONP. During the calcination process, the irreversible agglomeration of the MgO nanoparticles takes place. Therefore, only aggregated nanoparticles can be seen under SEM. A similar issue was reported with other metal oxide nanoparticles such as MnO_2. [60,]

Thermal properties of the MONP and MONP-GO samples were studied using differential thermogravimetry (DTG) and high-resolution thermogravimetry (TG). TG and DTG profiles of MONP and MONP-GO samples are shown in Figures 8 left and right panels, respectively. Three distinct thermal events were observed in the temperature ranges at 25-100 °C, 300-410 °C, and 600-670 °C (see Figure 8 left and right panels). The first and second events at 25-100 °C and 300-410 °C are due to the evaporation of physically adsorbed water and dehydroxylation of OH groups present on MgO nanoparticles. The peak observed at 630-680 °C is for MONP corresponding to the conversion of hydrated magnesium into oxide forms. Note that upon the incorporation of MgO nanoparticle into GO, peak at 630-680 °C is slightly shifted to lower temperature (see Figure 8 right

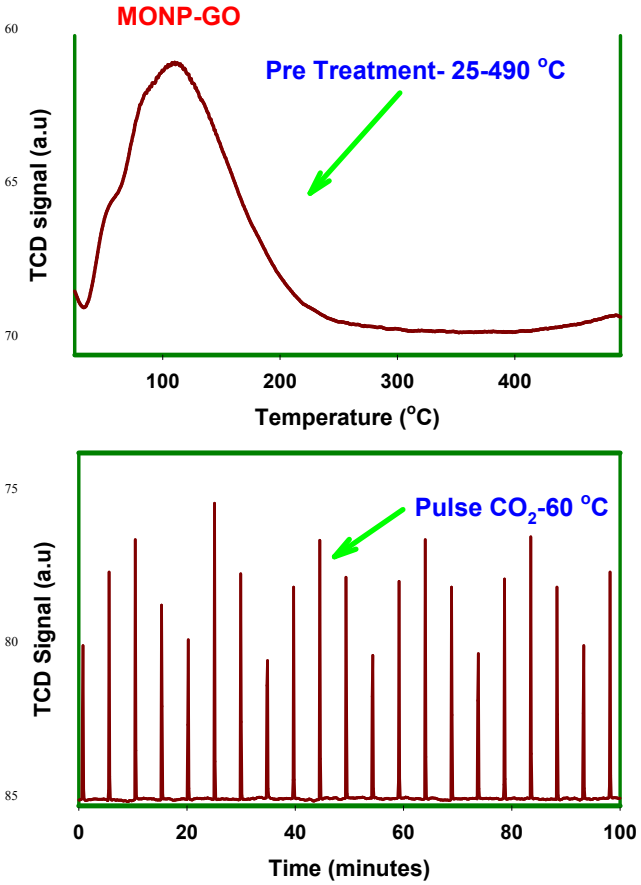

Figure 10. Pulse (60 °C) (bottom panel) and CO_2 pre-treatment (top panel) profiles recorded on the MONP-GO sample.

panels). This is due to the calcination of GO before the conversion of hydrated magnesium into their oxide forms. The amounts of MgO nanoparticles left after the thermal degradation are 65 % and 57 % for MONP and MONP-GO, respectively (see Figure 8 left panel). Thermogravimetric information reveals the high thermal stability of MONP and MONP-GO and their suitability to use at elevated temperatures.

N_2 adsorption isotherms measured at -196 °C for MONP and MONP-GO are depicted in Figure 9 left panel. To calculate Pore size distributions (PSD), adsorption branches of N_2 adsorption–desorption isotherms were treated with the 2DNLDFT (2DNLDFT is a Heterogeneous Surface model used for carbon materials implemented in SAIEUS program provided by Micromeritics).

N_2 adsorption isotherm obtained for both MONP and MONP-GO samples represents a typical type IV isotherm with a different hysteresis loop typical for mesoporous materials. A broad capillary condensation-evaporation step was observed for these samples beginning at a relative pressure of ~0.80-0.90.

NP and MONP-GO samples exhibit type IV isotherm with a broad H3 type hysteresis loop featuring narrow hysteresis loops distinct for slit-like pores or aggregates of plate-like particles

View Article Online
DOI: 10.1039/C9EN01442J

assembled into slit-like pores. The structural parameters calculated using N_2 sorption data are tabulated in Table 1.

A change in surface properties was observed upon the introduction of MONP onto GO, which significantly contributes to the decrease of the monolayer capacity, single point pore volume, mesopore volume, and surface area. For example, the MONP sample shows the surface area and total pore volume of 18 m^2/g and ~ 0.14 cm^3/g, and these values are reduced to 12 m^2/g and 0.10 cm^3/g, respectively, with the introduction of GO (Table 1). Figure 9 right panel shows the pore size distribution (PSD) curves for both MONP and MONP-GO samples. The PSD curves for both samples show the bi-model distribution and indicate the presence of a higher volume of mesopores compare to that of micropores. Both samples did not possess a significant volume of micropores (<0.01 cm^3/g) and thus, exhibit relatively low specific surface area (S_{BET}) (<20 m^2/g).

CO_2 Chemisorption

Figure 10 shows the CO_2 sorption isotherms of MONP and MONP-GO samples at elevated temperatures (60 &120 °C). Note that upon thermal treatment above 120 °C, commercially available amines (typically liquid amines or amine derived organosilica solid sorbents) tend to decompose. Therefore, it is problematic to use them for carbon dioxide sorption at elevated temperatures. The thermogravimetric studies discourse above explains that the MONP and MONP-GO structures are thermally stable even up to 600 °C and hence can be used for the CO_2 sorption at elevated temperatures. TPD (Temperature Programmed Desorption) measurement was employed to evaluate CO_2 uptake of the MONP and MONP-GO samples studied at 60 and 120 °C. MONP and MONP-GO composite materials were first subjected to pre-treatment under inert helium gas using a temperature ramp of 25 °C to 490 °C to remove all surface-bound impurities followed by cooling down to 120 °C (see Figure 10). After that, materials were exposed to a pulse of CO_2 at two different temperatures (60 °C and 120 °C). Materials were subsequently exposed to desorption by heating temperature up to 490 °C. Note that this desorption temperature (490 °C) is selected based on the calcination temperature observed in the range of 600-680 °C in TG studies described above (Figure 8).

Table 2. CO_2 uptake for the MONP and MONP-GO materials studied at 0, 25, 60, and 120 °C

Content	M C S at 0 °C (mmol/g)	M C S at 25 °C (mmol/g	M C S at 60 °C (mmol/g)	MCS at 120 °C (mmol/g))	CO_2 uptake at 60 °C mmol / atom of Mg	CO_2 uptake at 120 °C mmol / atom of Mg
MONP	0.22	0.20	2.97	2.79	1.97×10^{-22}	1.85×10^{-22}
MONP-GO	0.18	0.16	3.34	3.01	2.22×10^{-22}	2.00×10^{-22}

M C S: Maximum CO_2 Sorption

The most of CO_2 captured onto the basic active sites of MgO nanoparticles and MgO nanoparticles fabricated GO at 60 and 120 °C were desorbed mostly in the temperature range of ~365-367 °C and 366-367 °C, respectively (see Figure 11 left and right panel).

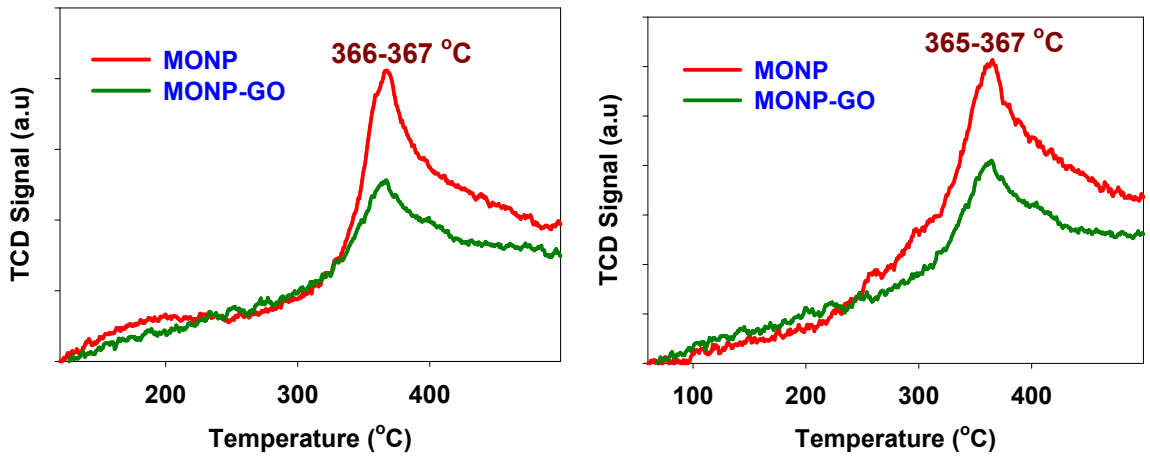

Figure 11. CO_2 TPD [left panel- pulse at 120 °C /right panel-pulse at 60 °C] profiles recorded for the MONP and MONP-GO samples studied.

View Article Online
DOI: 10.1039/C9EN01442J

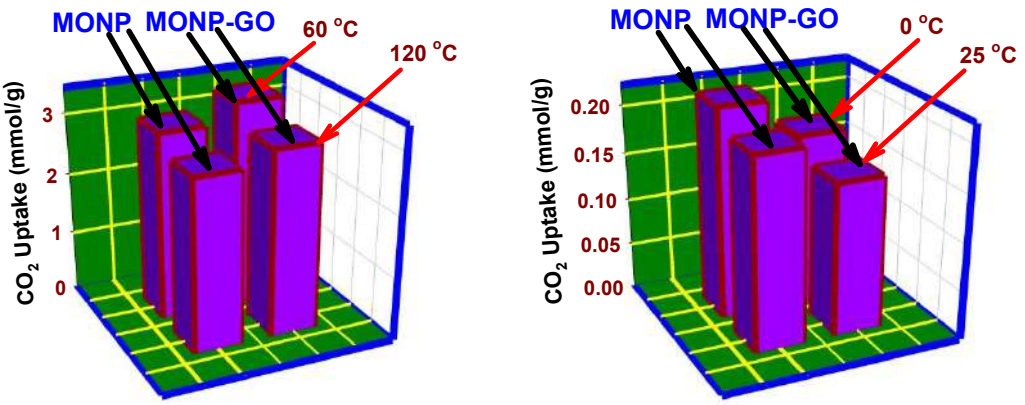

Figure 12. Left panel: CO_2 uptake changes for MONP and MONP-GO samples at 60 and 120 °C; (chemisorption). Right panel: CO_2 uptake changes MONP and MONP-GO samples at 0 and 25 °C; (physisorption).

TPD profile reveals the strength of basic sites present on MONP and MONP-GO samples. Note that the peaks centered at 366 °C are much broader upon CO_2 adsorption, which can be possibly due to the wide range of basic sites accountable for the formation of $MgCO_3$ upon reacting MONP with CO_2.

As can be seen from Table 2, upon fabricating MONP into the GO, there is a significant increase in the CO_2 uptake at 60 and 120 °C. For instance, MONP displays the CO_2 uptake of 2.97 mmol/g at 60 °C which is increased to 3.34 mmol/g for MONP-GO sample (see Table 2, Figure 12 left panel). Chemisorption at elevated temperatures (60 and 120 °C) relies on the surface functionalization of the material over porosity. When graphite is converted to graphene oxide (GO) (see Scheme 2a), hydroxyl (-OH) functional groups are generated. These -OH groups involved in the increased CO_2 sorption at elevated temperatures. For instance, CO_2 adsorption capacity of MONP and MONP-GO at 60 °C is 2.97 mmol/g, and 3.34 mmol/g, respectively. The amounts of adsorbed CO_2 per atom of Mg for both MONP and MONP-GO have been calculated and given in Table 1. CO_2 uptake for MONP and MONP-GO at 60 °C is higher than their respective CO_2 uptakes at 120 °C. This is due to the exothermic adsorption of CO_2 onto solid sorbents resulting in a decrease in the adsorption capacity at high temperatures.

Note that CO_2 uptake obtained for the MONP sample at 60 and 120 °C was caused by CO_2 sorption on both magnesium species and hydroxyl groups present in MONP. The ffabrication of MONP onto the GO (MONP-GO) further increases the number of hydroxyl groups and thus responsible for higher CO_2 uptake at elevated temperatures. These phenomena can be further explained by the existence of three different types (the terminal, bi-bridged, and

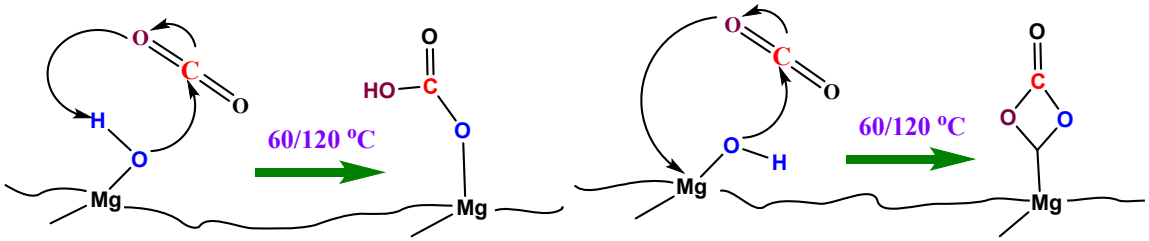

Scheme 3. Systematic illustration of possible hydrogen carbonate (left panel) and bidentate carbonate (right panel) formation upon CO_2 chemisorption on either MONP or MONP-GO samples

View Article Online
DOI: 10.1039/C9EN01442J

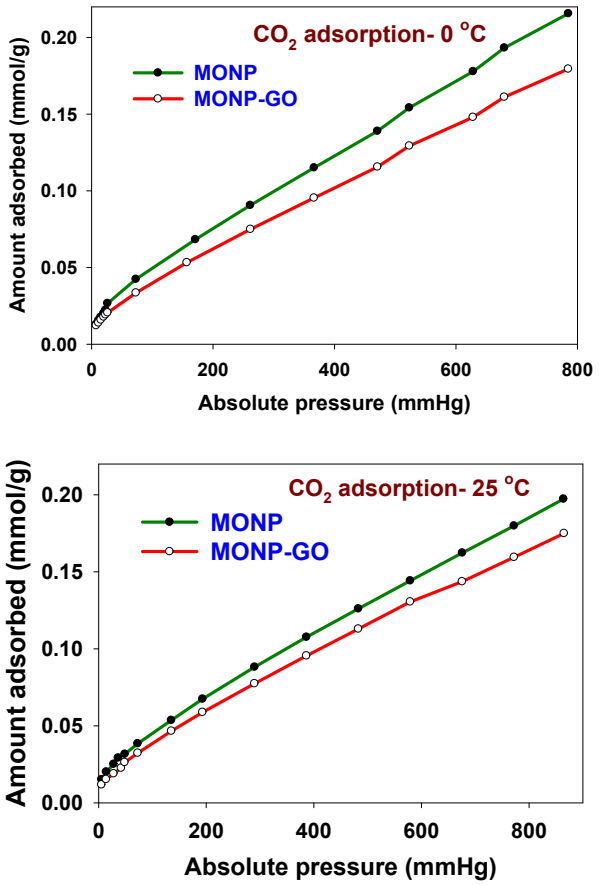

Figure 13. CO_2 adsorption isotherms at 0°C (top panel) and at 25 °C (bottom panel) measured on the MONP and MONP-GO samples studied.

tri-bridged,) of hydroxyl groups available on magnesium oxide surface even at 600 °C which consequently enhance the CO_2 chemisorption[61]. Terminal OH groups available in MONP and MONP-GO are responsible to form hydrogen carbonate species upon CO_2 sorption (see illustration in Scheme 3 left panel)[57-60]. Secondly, acid-base pair sites present in magnesium (Mg^{2+}-O^{2-}) surface form bidentate carbonate complexes (see Scheme 3 right panel) [62-65]. Acidic (Mg^{2+}) and basic (O^{2-}) sites on the surface of the MONP and MONP-GO could also effectively increase the CO_2 sorption capacity. Here, it is possible to donate electrons from oxygen atoms of CO_2 (Lewis base) to the Mg^{2+} (Lewis acid) as illustrated in Scheme 3 right panel and thus create a very favorable atmosphere for CO_2 chemisorption. The formation of hydrogen carbonate and bidentate carbonate adducts upon CO_2 adsorption onto metal oxides including alumina (Al_2O_3), zirconia (ZrO_2), and Al_2O_3/ZrO_2 surface at elevated temperatures is well established and shown in the literature using FTIR analysis [62, 64-66].

Following is a summary of CO_2 sorption capacities reported previously for metal-based sorbents at elevated temperatures. CO_2 sorption capacities recorded using a metal-organic framework (MOF), zeolite-based sorbents, amine-functionalized solid sorbents, hybrid inorganic metal oxides at elevated temperatures (≥ 60 °C) are listed in Table 3. For instance, Cai and co-workers studied alumina with metal oxide (Ca, Mg, Ce, Cu, and Cr) supported hybrid materials for CO_2 sorption at 120 °C [67] and reported the highest CO_2 uptake of 1.80 mmol/g. Zulfiqur et al investigated the CO_2 sorption on amidoxime-based materials at high pressure and selected temperature (180 bar and 70 °C) and showed the highest CO_2 uptake of 2.71 mmol/g [68]. CO_2 adsorption on sodium-based sorbents at 315 °C was investigated by Siriwardena and co-workers and reported the maximum CO_2 uptake of 3 mmol/g [69]. Siriwardena et al further worked on zeolite-based solid sorbents for CO_2 sorption at 120 °C. They reported the highest CO_2 sorption capacity of 0.7 (1 bar pressure) and 1.2 mmol/g (20 bar pressure) [61]. CO_2 sorption on MgO/Al_2O_3 composite in the presence and absence of water was studied by Li and co-workers [70]. Under hydrous and anhydrous conditions, they reported maximum CO_2 uptake of about 0.97 and 1.36 mmol/g, respectively. Sorption studies on three main composites, namely isocyanurate-based organosilica-alumina, mesoporous alumina-zirconia-organosilica, and amidoxime functionalized mesoporous, respectively, displayed the maximum CO_2 uptake of 2.20, 3.07, and 3.02 mmol/g at 120 °C [39, 66, 71]. Nano-structured $MgO-Al_2O_3$ aerogel at 200 °C was studied by Han and co-workers and reported the maximum CO_2 uptake of 0.97 mmol/g [72]. Polyethyleneimine (PEI) impregnated mesoporous silica for CO_2 sorption at 75 °C was investigated by Song et al. With 75 wt% of PEI loading on mesoporous silica, it adsorbed maximum CO_2 uptake of about 3.02 mmol/g [73]. CO_2 uptake on hydrotalcite-like compounds such as MgAlO, CaAlO, CoAlO, and CaCoAlO at 350 °C was investigated by Wang et al and showed the CO_2 uptake values changed from 0.87 to 1.39 mmol/g with respect to different hydrotalcite precursors used in the synthesis [74]. A mixture of

Table 3. Comparison of CO_2 uptake values obtained at different temperatures: current work with various solid sorbents reported in literature.

Material	Sorption Temperature (°C)	Maximum CO_2 Uptake (mmol/g)	Reference
Hybrid Al-metal oxides (Ca, Mg, Ce, Cu, Cr)	120	1.80	[67]
Acetamidoxime/polyamidoxime	70	2.71	[68]
Sodium based sorbents	315	3.02	[69]
Zeolite based sorbents	120	1.20	[61]
MgO/Al_2O_3composites	60	1.36	[70]
Al incorporated organosilica	120	2.20	[71]
Alumina zirconia silica composites	60	3.02	[66]

View Article Online
DOI: 10.1039/C9EN01442J

Alumina zirconia silica composites	120	2.76	[66]
Amidoxime modified mesoporous silica	120	3.07	[39]
MgO-Al_2O_3 aerogel	200	0.97	[72]
PEI impregnated MCM 41	75	3.02	[73]
Mixed oxide of Ca, Al, Co, Mg (Hydrotalcite)	350	1.39	[74]
$K_2CO_3/MgO/Al_2O_3$	60	2.49	[75]
MONP	60/120	2.97/2.79	This work
MONP-GO	60/120	3.34/3.01	This work

$K_2CO_3/MgO/Al_2O_3$ metal oxides for CO_2 uptake at 60 °C was investigated by Li et al and displayed the maximum CO_2 capacity of 2.49 mmol/g [75]. In our current work, CO_2 sorption capacity recorded for MONP and MONP-GO are comparatively higher than the aforementioned studies listed in Table 3.

In addition to CO_2 chemisorption measurement at 60 and 120 °C, CO_2 physisorption at low temperatures (0 and 25 °C and 760 mmHg pressure conditions) was also investigated. Figure 13 left and right panel displays the CO_2 uptake measured on MONP and MONP-GO samples at 0 and 25 °C. respectively. CO_2 adsorption capacities recorded at 0 and 25 °C are listed in Table 2. As can be seen from Table 2 and Figure 12 right panel, CO_2 uptake recorded for MONP and MONP-GO at low temperatures is significantly lower as compared to those recorded at elevated temperatures.

Note that low temperature CO_2 sorption mainly occurs through the physisorption mechanism. The samples with higher microporosity show higher CO_2 uptake at ambient or low temperature conditions. For instance, MONP possesses microporous volume <0.01 cm^3/g and thus displays CO_2 uptake of about 0.22 mmol/g at 0 °C and 0.18 mmol/g at 25 °C (Table 2 and Figure 12 right panel). Although CO_2 uptake at elevated temperatures is higher for MONP-GO as compared with that of MONP; values recorded at low temperatures are in the reverse order. This is due to the slight reduction of surface properties upon fabricating MgO nanoparticle on GO.

Conclusions

This study demonstrates the successful synthesis of MgO nanoparticle decorated GO nanocomposite via a one-pot synthesis method using low cost and naturally abundant resources including dolomite, bittern, and graphite. Materials were examined for CO_2 sorption at low (0 °C), ambient (25 °C), and elevated temperatures (60 °C and 120 °C). Both MONP and MONP-GO acts as weak physical sorbents of CO_2 at low and ambient temperatures. MONP-GO showed the highest CO_2 uptake of 3.34 mmol/g at 60 °C and 3.01 mmol/g at 120 °C, respectively. Due to high thermal and chemical stability, low-cost, and environmentally benignity, these materials show potential in industrial-scale CO_2 sorption at elevated temperatures.

Acknowledgment

The authors are grateful to the financial support from National science foundation Grant no. TG/2016/Tec-D/02. Also, like to thankful to technical staff of new environmental laboratory, Department of Civil Engineering, Faculty of Engineering, University of Peradeniya. The authors would also like thank Prof. Mietek Jaroniec from Department of Chemistry, Kent State University for providing support with the CO_2 chemisorption, physisorption, thermogravimetric and gas sorption measurements facilities and analysis.

Conflicts of interest

There are no conflicts to declare

References

1. E.C Alfredsson, Green consumption—no solution for climate change. Energy, **2004**, *29*, 513-524;

2. S. B. Fredriksen and K.-J. Jens, Oxidative Degradation of Aqueous Amine Solutions of MEA, AMP, MDEA, Pz: A Review. Energy Procedia, **2013**, *37*, 1770-1777;

3. F. Vega, B. Navarrete, M. Cano and E. Portillo, Development of Partial Oxy-combustion Technology: New Solvents Applied to CO_2 Capture in Fossil-fuels Power Plants. Energy Procedia, **2014**, *63*, 484-489;

4. R. Dassanayake, C. Gunathilake, A. Noureddine and M. Jaroniec, Amidoxime-functionalized nanocrystalline cellulose–mesoporous silica composites for carbon dioxide sorption at ambient and elevated temperatures. J. Mater. Chem. A, **2017**, *5*, 7462-7473;

5. C. Gunathilake, R. Dassanayake, A. Noureddine and M. Jaroniec, Amidoxime-functionalized microcrystalline cellulose–mesoporous silica composites for carbon dioxide sorption at elevated temperatures. J. Mater. Chem. A, **2016,** *4*, 4808-4819;

6. G. T. Rochelle, Amine Scrubbing for CO_2 Capture. Science, **2009**, *325*,1652-1654;

7. A. H. Berger and A.S. Bhown, Comparing physisorption and chemisorption solid sorbents for use separating CO_2 from flue gas using temperature swing adsorption. Energy Procedia, **2011**, *4*, 562-567;

8.A. Samanta, A. Zhao, G. K. H. Shimizu, P. Sarkar and R. Gupta, Post-Combustion CO_2 Capture Using Solid Sorbents: A Review. Ind. Eng. Chem. Res., **2012**, *51*, 1438-1463;

9. L. Cai, J. Chen, Z. Liu, H. Wang, H. Yang and W. Ding, Magnesium Oxide Nanoparticles: Effective Agricultural Antibacterial Agent Against Ralstonia solanacearum. Front. Microbiol., **2018**, *9*, 790-796;

10. C. Aksel, P. D. Warren and F. L. Riley, Fracture behaviour of magnesia and magnesia–spinel composites before and after thermal shock. J. Eur. Ceram. Soc, **2004,** *24*, 2407-2416;

11. Z. Hu, W. Zhang, H. He, Y. Feng and S. Da, Preparation of magnesia-zirconia based mimetic biomembrane stationary phase and its applications in evaluating drug-membrane interactions. Chinese J. Chromatogr. A, **2008**, *26*, 529-533;

12. H. W. Choi, S. Y. Kim, W. K. Kim and J. Lee, Enhancement of electron injection in inverted top-emitting organic light-emitting diodes using an insulating magnesium oxide buffer layer. Appl Phys Lett., **2005**, *87*, 082102- 082103;

View Article Online
DOI: 10.1039/C9EN01442J

13. T. Yano, H. Matsui, T. Koike, H. Ishiguro, H. Fujihara, M. Yoshihara and T. Maeshimaa, Magnesium oxide-catalysed reaction of carbon dioxide with an epoxide with retention of stereochemistry. ChemComm, **1997**, *12*, 1129-1130;

14. A. Kay and M. Grätzel, Dye-Sensitized Core−Shell Nanocrystals: Improved Efficiency of Mesoporous Tin Oxide Electrodes Coated with a Thin Layer of an Insulating Oxide. Chem. Mater., **2002**, *14*, 2930-2935;

15. M. Sain, S. Park, F. Suhara and S. Law, Flame retardant and mechanical properties of natural fibre–PP composites containing magnesium hydroxide. Polym. Degrad. Stab., **2004**, *83*, 363-367;

16. O. Baidukova and E.V. Skorb, Ultrasound-assisted synthesis of magnesium hydroxide nanoparticles from magnesium. Ultrasonics Sonochemistry, **2016**, *31*, 423-428;

17. Y. Ding, G. Zhang, H. Wu, B. Hai, L. Wang and Y. Qian, Nanoscale Magnesium Hydroxide and Magnesium Oxide Powders: Control over Size, Shape, and Structure via Hydrothermal Synthesis. Chem. Mater., **2001**, *13*, 435-440;

18. C. Y. Tai, C. T. Tai, M. H. Chang and H. S. Liu, Synthesis of Magnesium Hydroxide and Oxide Nanoparticles Using a Spinning Disk Reactor. Ind. Eng. Chem. Res., **2007**, *46*, 5536-5541;

19. R. Portillo, T. Lopez, R. Gomez, A. Bokhimi Morales and O. Novaro, Magnesia Synthesis via Sol−Gel: Structure and Reactivity. Langmuir, **1996**, *12*, 40-44;

20. M. S. Mastuli, N. Kamarulzaman, M. Nawawi, A. Mahat, R. Rusdi and N. Kamarudin, Growth mechanisms of MgO nanocrystals via a sol-gel synthesis using different complexing agents. Nanoscale Res. Lett., **2014**, *9*, 134-140;

21.S. Wang, M. Yi and Z. Shen, The effect of surfactants and their concentration on the liquid exfoliation of graphene. RSC Adv., **2016**, *6*, 56705-56710;

22 M. S. Mastuli, N. S. Ansari, M. A. Nawaw and A. M. Mahat, Effects of Cationic Surfactant in Sol-gel Synthesis of Nano Sized Magnesium Oxide. APCBEE Procedia, **2012,** *3*, 93-98;

23. S. Balamurugan, L. Ashna and P. Parthiban, Synthesis of Nanocrystalline MgO Particles by Combustion Followed by Annealing Method Using Hexamine as a Fuel. J. Nanotechnol., **2014**, *2014*, 1-6;

24. C. N. Rao, A. K. Sood, K. S. Subrahmanyam and A. Govindaraj, Graphene: the new two-dimensional nanomaterial. Angew. Chem. Int. Ed. Engl., **2009**, *48*, 7752-7777;

25 J. Sun, N. Yang, Z. Sun, M. Zeng, L. Fu, C. Hu and S. Hu, Fully Converting Graphite into Graphene Oxide Hydrogels by Preoxidation with Impure Manganese Dioxide. ACS Appl. Mater. Interfaces, **2015**, *7*, 21356-21363;

26. J. Pokhrel, N. Bhoria, S. Anastasiou, T. Tsoufis, D. Gournis, G. Romanos and G. N. Karanikolos, CO_2 adsorption behavior of amine-functionalized ZIF-8, graphene oxide, and ZIF-8/graphene oxide composites under dry and wet conditions. Microporous Mesoporous Mater., **2018**, *267*, 53-67;

27. D. Chen, H. Feng and J. Li, Graphene Oxide: Preparation, Functionalization, and Electrochemical Applications. Chem. Rev., **2012**, *112*, 6027-6053;

28. M. Karabörk, R. Maher Zubair, S. Uruş and M. Tümer, Synthesis and characterization of graphene oxide-based hybrid ligand and its metal complexes: Highly efficient sensor and catalytic properties. Appl. Organomet. Chem., **2018**, *32*, 1-12;

29. Y. Dong, J. Li, L. Shi, J. Xu, X. Wang, Z. Guo and W. Liu, Graphene oxide–iron complex: synthesis, characterization and visible-light-driven photocatalysis. J. Mater. Chem. A, **2013**, *1*, 644-650;

30 S. Luanwuthi, A. Krittayavathananon, P. Srimuk and M. Sawangphruk, In situ synthesis of permselective zeolitic imidazolate framework-8/graphene oxide composites: rotating disk electrode and Langmuir adsorption isotherm. RSC Adv., **2015**, *5*, 46617-46623;

31. A. K. Mishrand and S. Ramaprabhu, Carbon dioxide adsorption in graphene sheets. AIP Adv., **2011,** *1*, 032152;

32. R. Kumar, K. Jayaramulu, T. K. Maji and C. N. R. Rao, Hybrid nanocomposites of ZIF-8 with graphene oxide exhibiting tunable morphology, significant CO_2 uptake and other novel properties. ChemComm, **2013**, *49*, 4947-4949;

33. P. Bhanja, S. K. Das, A. K. Patra and A. Bhaumik, Functionalized graphene oxide as an efficient adsorbent for CO_2 capture and support for heterogeneous catalysis. RSC Adv., **2016**, *6*, 72055-72068;

34. F. Zhou, H. N. Tien, Q. Dong, W. L. Xu, H. Li, S. Li and M. Yu, Ultrathin, ethylenediamine-functionalized graphene oxide membranes on hollow fibers for CO_2 capture. J. Membr. Sci, **2019**, *573*, 184-191;

35. A. Alghamdi, A. Alshahrani, N. Khdary, F. Alharthi, H. Alattas and S. Adil, Enhanced CO_2 Adsorption by Nitrogen-Doped Graphene Oxide Sheets (N-GOs) Prepared by Employing Polymeric Precursors. Materials, **2018**, *11*, 578-584;

36. S. Yang, , L. Zhan, X. Xu, Y. Wang, L. Ling and X. Feng, Graphene-Based Porous Silica Sheets Impregnated with Polyethyleneimine for Superior CO_2 Capture. Adv. Mater., **2013**, *25*, 2130-2134;

37.International, A., ASTM D1298-12b(2017), Standard Test Method for Density, Relative Density, or API Gravity of Crude Petroleum and Liquid Petroleum Products by Hydrometer Method, ASTM International, West Conshohocken, PA, 2017, www.astm.org. **2017**;

38.International, A., Standard Test Method for Density in Relative Density (Specific Gravity), or API Gravity of Crude Petroleum and Liquid Petroleum Products. **2003**, 221;

39. C. Gunathilake and M. Jaroniec, Mesoporous Organosilica with Amidoxime Groups for CO_2 Sorption. ACS Appl. Mater. Interfaces, **2014**, *6*, 13069-13078;

40. H. T. Schaef, C. F. Windisch, B. P. McGrail, P. F. Martin and K. M Rosso, Brucite [$Mg(OH_2)$] carbonation in wet supercritical CO2: An in situ high pressure X-ray diffraction study. Geochim. Cosmochim. Acta, **2011**, *75*, 7458-7471;

41. M. A. Aramendía, J. A. Benítez, V. Borau, C. Jiménez, J. M. Marinas, J. R. Ruiz and F. Urbano, Study of MgO and Pt/MgO Systems by XRD, TPR, and ^{1}H MAS NMR. Langmuir, **1999**, *15*, 1192-1197;

42. X.-F. Wu, G.-S. Hu, B.-B. Wang and Y.-F. Yang, Synthesis and characterization of superfine magnesium hydroxide with monodispersity. J. Cryst. Growth, **2008**, *310*, 457-461;

43. X. Zeng, J. Yang, L. Zhang, L. Chen and W. Yuan, Homogeneous dispersion of high-conductive reduced graphene oxide sheets for polymethylmethacrylate nanocomposites. Powder Diffr., **2014**, *29*, 241-247;

44. S. Chaudhary, P. Sharma, R. Kumar and S. K. Mehta, Nanoscale surface designing of Cerium oxide nanoparticles for controlling growth, stability, optical and thermal properties. Ceramics International, **2015,** *41*, 10995-11003;

45. Q. Jia, H. Han, L.Wang, B. Liu, H. Yang and J. Shen, Effects of CTAC micelles on the molecular structures and separation performance

View Article Online
DOI: 10.1039/C9EN01442J

of thin-film composite (TFC) membranes in forward osmosis processes. Desalination, **2014**, *340*, 30-41;

46. G. Lu, S. Mao, S. Park, R. S. Ruoff and J. Chen, Facile, noncovalent decoration of graphene oxide sheets with nanocrystals. Nano Res., **2009**, *2*, 192-200;

47. F. Y Ban, S. R. Majid, H. N. Ming and H. Lim, Graphene Oxide and Its Electrochemical Performance, Int. J. Electrochem. Sci., **2012**, *7*, 4345 – 4351.

48. F. T. Johra, J.W. Lee and W. G. Jung, Facile and safe graphene preparation on solution-based platform, Journal of Industrial and Engineering Chemistry, **2014**, *20*, 2883-2887

49. C. Valencia, C.H. Valencia, F. Zuluaga, M.E. Valencia, J.H. Mina, C.D. Grande-Tovar, Synthesis and Application of Scaffolds of Chitosan-Graphene Oxide by the Freeze-Drying Method for Tissue Regeneration. Molecules **2018**, *23*, 2651

50. C. W. Wong, Y. S. Chan, J. Jeevanandam, K. Pal, M. Bechelany, M. A. Elkodous and G. S. El-Sayyad, Response Surface Methodology Optimization of Mono-dispersed MgO Nanoparticles Fabricated by Ultrasonic-Assisted Sol–Gel Method for Outstanding Antimicrobial and Antibiofilm Activities, J. Clus. Sci., **2019**

51. H. Wang, J. T. Robinson, X. Li and H. Dai, Solvothermal Reduction of Chemically Exfoliated Graphene Sheets, J. Am. Chem. Soc, **2009**, *131*, 9910-9911;

52. H. Kuleci, C. Schmidt, E. Rybacki, G. Dresen and R. Abart, Mechanical effects of the hydration of periclase to brucite in calcite-periclase aggregates; an experimental study. European Geosciences Union General Assembly Conference at Vienna, **2013**, 7706;

53. J. Oviedo, C.J. Calzado and J.F. Sanz, Molecular dynamics simulations of the MgO(001) surface hydroxylation. J. Chem. Phys., **1998**, *108*, 4219-4225;

54. M. Heidarizad and S. Sevinç Şengör Graphene Oxide/Magnesium Oxide Nanocomposite: A Novel Catalyst for Ozonation of Phenol from Wastewater. World Environmental and Water Resources Congress, **2017**, 192-200;

55. M. Heidarizad and S.S. Şengör, Synthesis of graphene oxide/magnesium oxide nanocomposites with high-rate adsorption of methylene blue. J. Mol. Liq., **2016**, *224,* 607-617;

56. M. P. Beck, Y. Yuan, P. Warrier and A. S. Teja, The thermal conductivity of alumina nanofluids in water, ethylene glycol, and ethylene glycol + water mixtures. J. Nanoparticle Res., **2010**, *12*, 1469-1477;

57. R. J. Qi and Y. J. Zhu, Microwave-assisted synthesis of calcium carbonate (vaterite) of various morphologies in water-ethylene glycol mixed solvents. J. Phys .Chem. B, **2006**, *110*, 8302-8306;

58. Y. Chen, X. Ji and X. Wang, Microwave-assisted synthesis of spheroidal vaterite $CaCO_3$ in ethylene glycol–water mixed solvents without surfactants. J. Cryst. Growth, **2010**, *312*, 3191-3197;

59. D. Zhao, J. Jiang, J. Xu, L. Yang, T. Song and P. Zhang, Synthesis of template-free hollow vaterite $CaCO_3$ microspheres in the H_2O/EG system. Mater. Lett., **2013**, *104***,** 28-30;

60. R. S. Dassanayake, E. Rajakaruna, H. Moussa and N. Abidi, One-pot synthesis of MnO2–chitin hybrids for effective removal of methylene blue Int. J. Biol. Macromol., **2016**, *93*, 350-358

61. R. V. Siriwardane, M.-S. Shen, E. P. Fisher, and J. Losch, , Adsorption of CO_2 on Zeolites at Moderate Temperatures. Energ. Fuel, **2005,** *19*, 1153-1159;

62. B. Bachiller-Baeza, I. Rodriguez-Ramos and A. Guerrero-Ruiz, Interaction of Carbon Dioxide with the Surface of Zirconia Polymorphs. Langmuir, **1998**, *14*, 3556-3564;

63. W. Hertl, Surface chemistry of zirconia polymorphs. Langmuir, **1989**, *5*, 96-100;

64 C. Morterra, G. Cerrato, F. Pinna and M. Signoretto, Crystal Phase, Spectral Features, and Catalytic Activity of Sulfate-Doped Zirconia Systems. J. Catal., **1995**, *157*, 109-123;

65. K. Pokrovski, K.T. Jung and A.T. Bell, Investigation of CO and CO_2 Adsorption on Tetragonal and Monoclinic Zirconia, Langmuir, **2001**, 17, 4297-4303;

66. C. Gunathilake and M. Jaroniec, Mesoporous alumina–zirconia–organosilica composites for CO_2 capture at ambient and elevated temperatures. J. Mater. Chem. A, **2015**, *3*, 2707-2716;

67. W. Cai, J. Yu, C. Anand, A. Vinu and M. Jaroniec, Facile Synthesis of Ordered Mesoporous Alumina and Alumina-Supported Metal Oxides with Tailored Adsorption and Framework Properties. Chem. Mater., **2011**, *23*, 1147-1157;

68. S. Zulfiqar, F. Karadas, J. Park, E. Deniz, G. D. Stucky, Y. Jung, M. Atilhan and C. T. Yavuz, Amidoximes: promising candidates for CO_2 capture. Energy Environ. Sci., **2011**, *4*, 4528-4531;

69. R. V. Siriwardane, C. Robinson, M. Shen and T. Simonyi, Novel Regenerable Sodium-Based Sorbents for CO_2 Capture at Warm Gas Temperatures. Energ Fuel, **2007,** *21*, 2088-2097;

70. L. Li, X. Wen, X. Fu, F. Wang, N. Zhao, F. Xiao, W. Wei and Y. Sun, MgO/Al_2O_3 Sorbent for CO_2 Capture. Energ Fuel, **2010**, *24*, 5773-5780;

71. C. Gunathilake, M. Gangoda and M. Jaroniec, Mesoporous isocyanurate-containing organosilica–alumina composites and their thermal treatment in nitrogen for carbon dioxide sorption at elevated temperatures. J. Mater. Chem. A, **2013**, *1***,** 8244-8252;

72. S. J. Han, , Y. Bang, H. J. Kwon, H. C. Lee, V. Hiremath, I. K. Song, and J. G. Seo, Elevated temperature CO_2 capture on nano-structured $MgO–Al_2O_3$ aerogel: Effect of Mg/Al molar ratio. Chem. Engi. J., **2014,** *242*, 357-363;

73. X. Xu, C. Song, B. G. Miller and A. W. Scaroni, Influence of Moisture on CO_2 Separation from Gas Mixture by a Nanoporous Adsorbent Based on Polyethylenimine-Modified Molecular Sieve MCM-41. Ind. Eng. Chem. Res., **2005,** *44*, 8113-8119;

74. X. P. Wang, J. J. Yu, J. Cheng, Z. P. Hao and Z. P. Xu, High-Temperature Adsorption of Carbon Dioxide on Mixed Oxides Derived from Hydrotalcite-Like Compounds, Environ. Technol., **2008,** *42*, 614-618;

75. L. Li, X. Wen, X. Fu, F. Wang, N. Zhao, F. Xiao, W. Wei and Y. Sun., CO_2 Capture over $K_2CO_3/MgO/Al_2O_3$ Dry Sorbent in a Fluidized Bed. Energ Fuel, **2011,** *25***,** 3835-3842;

View Article Online
DOI: 10.1039/C9EN01442J

TOC Graphics

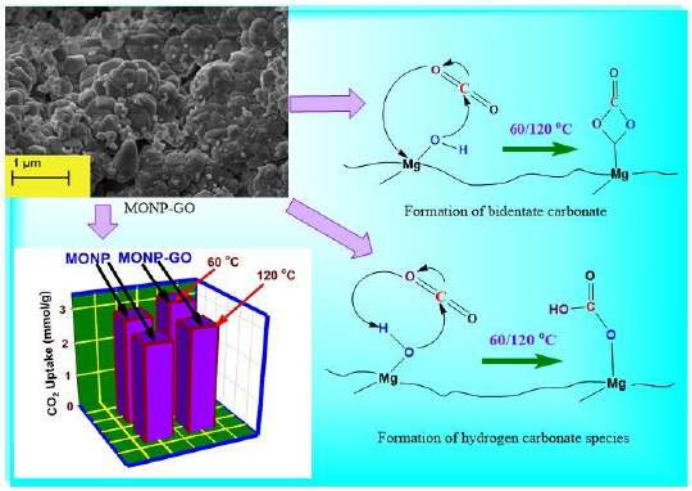

MONP and MONP-GO sorbents exhibited relatively high CO_2 sorption capacity (2.79-3.34 mmol/g) at elavated temperatures conditions.